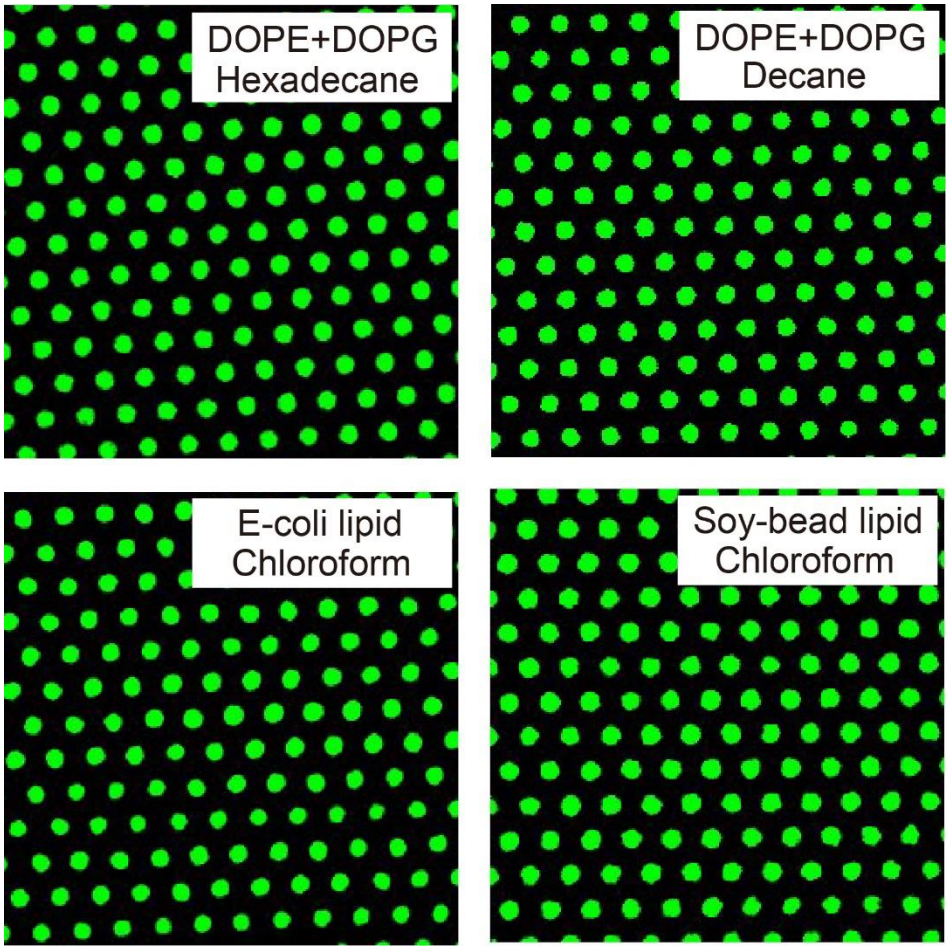

Supplementary Figure 1. Fluorescent image of ALBiCs using various organic solvents and lipids

Fluorescent image of Alexa 488 encapsulated into microchambers sealed by lipid membranes. Various types of organic solvents and lipid molecules; decane, hexadecane, soy-bean lipid (Sigma-Aldrich, USA), and total *Escherichia coli* lipid (Avanti Polar Lipids, USA), were used for membrane formation.

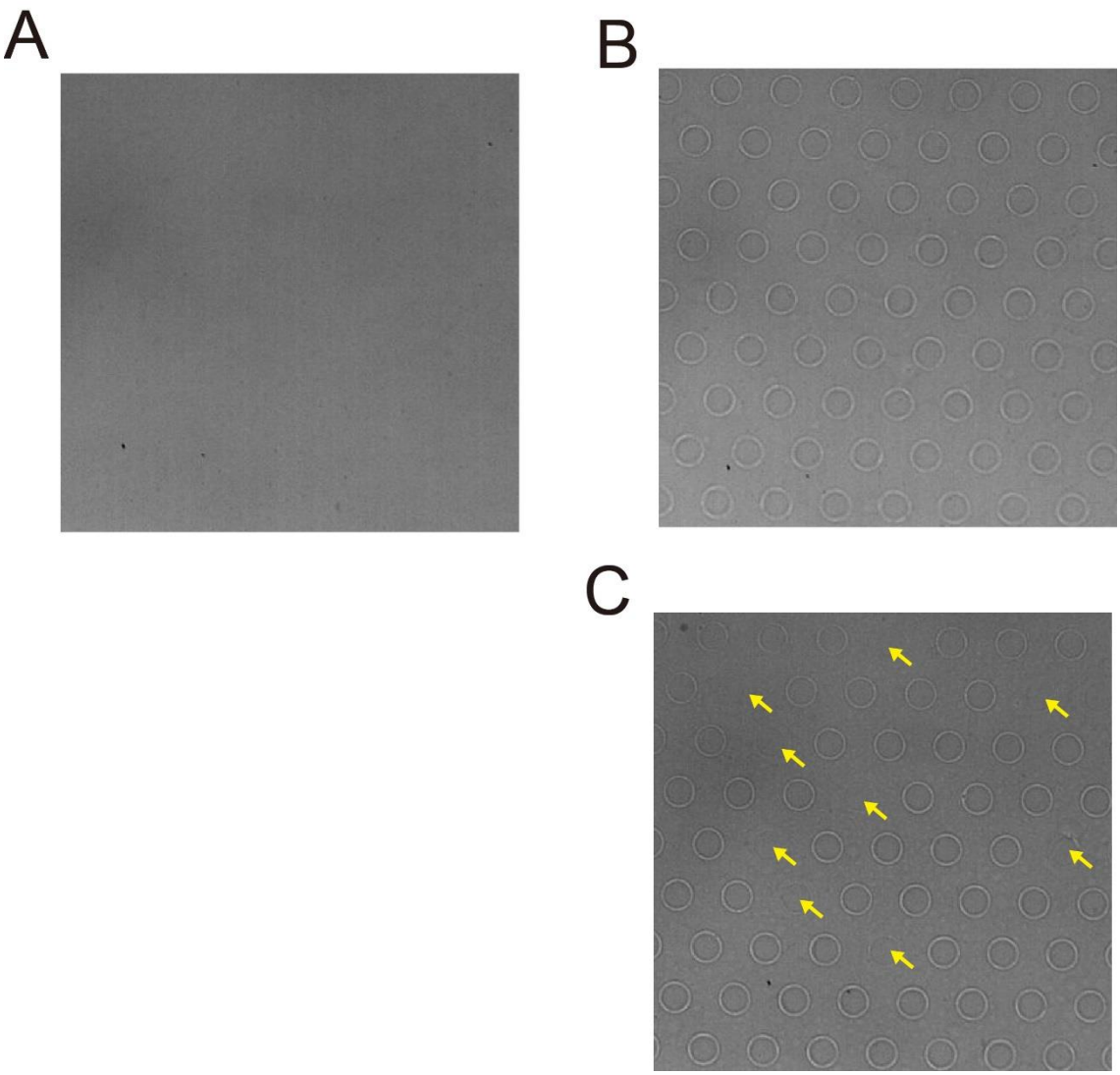

Supplementary Figure 2. Bright-field image of ALBiCs

Bright-field image of ALBiCs before (**A**) and after (**B, C**) lipid membrane formation. (**C**) is a rare image in which some chambers are not sealed with lipid membranes (yellow arrows).

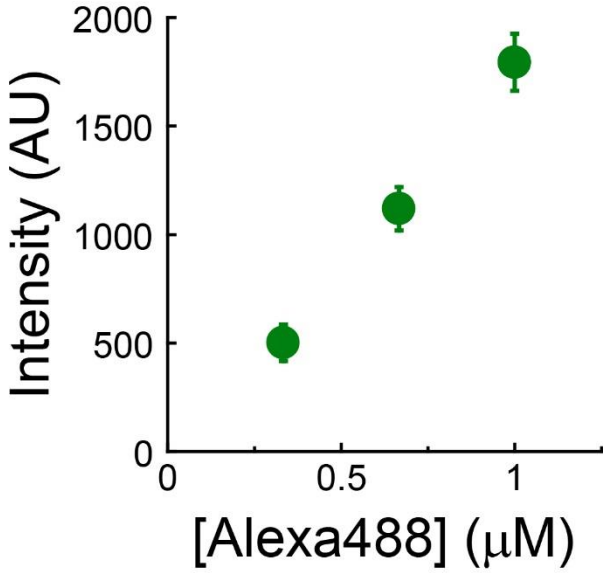

Supplementary Figure 3. Fluorescent intensity of Alexa488

Dependence of the fluorescent intensity of Alexa 488 on its concentration.

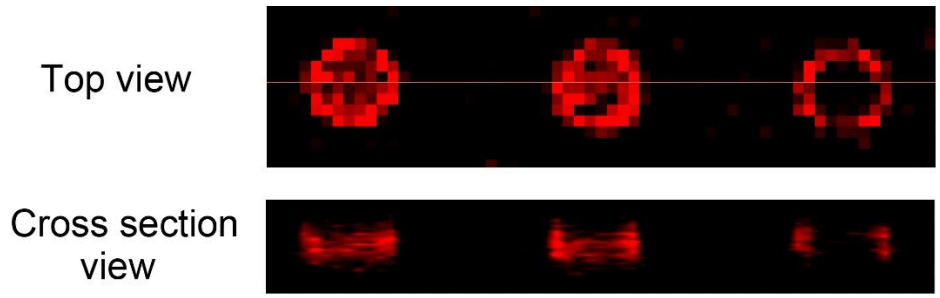

Supplementary Figure 4. 3D-imageing of RhP-M in micro-chamber

The fluorescent images of RhP-M in micro-chambers sealed with lipid membranes (left, middle) or that without sealing (right).

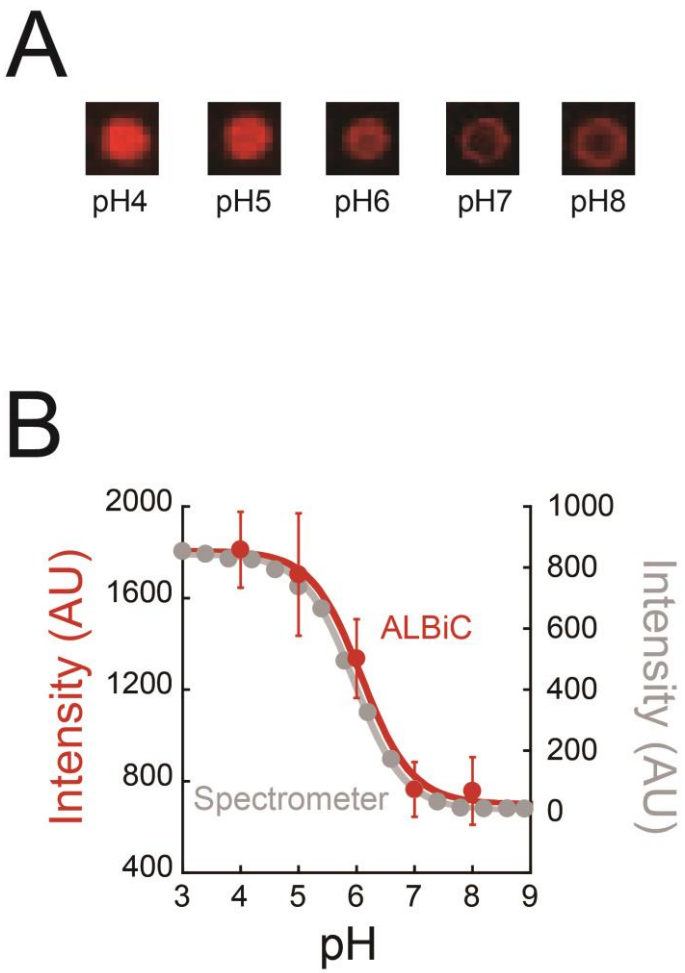

Supplementary Figure 5. Fluorescent intensity of RhP-M according to pH

(**A**) Fluorescent images of 10 μM RhP-M in the chambers recorded at pH 4–8. (**B**) Calibration curve of the fluorescent intensity using the ALBiC system (red) or a spectrometer (gray). The data were fitted with the function $y = C_1/(1 - 10^{(pH-pKa)}) + C_2$. p*K*a values were determined to be 6.0 for the ALBiC system and 6.0 for the spectrometer.

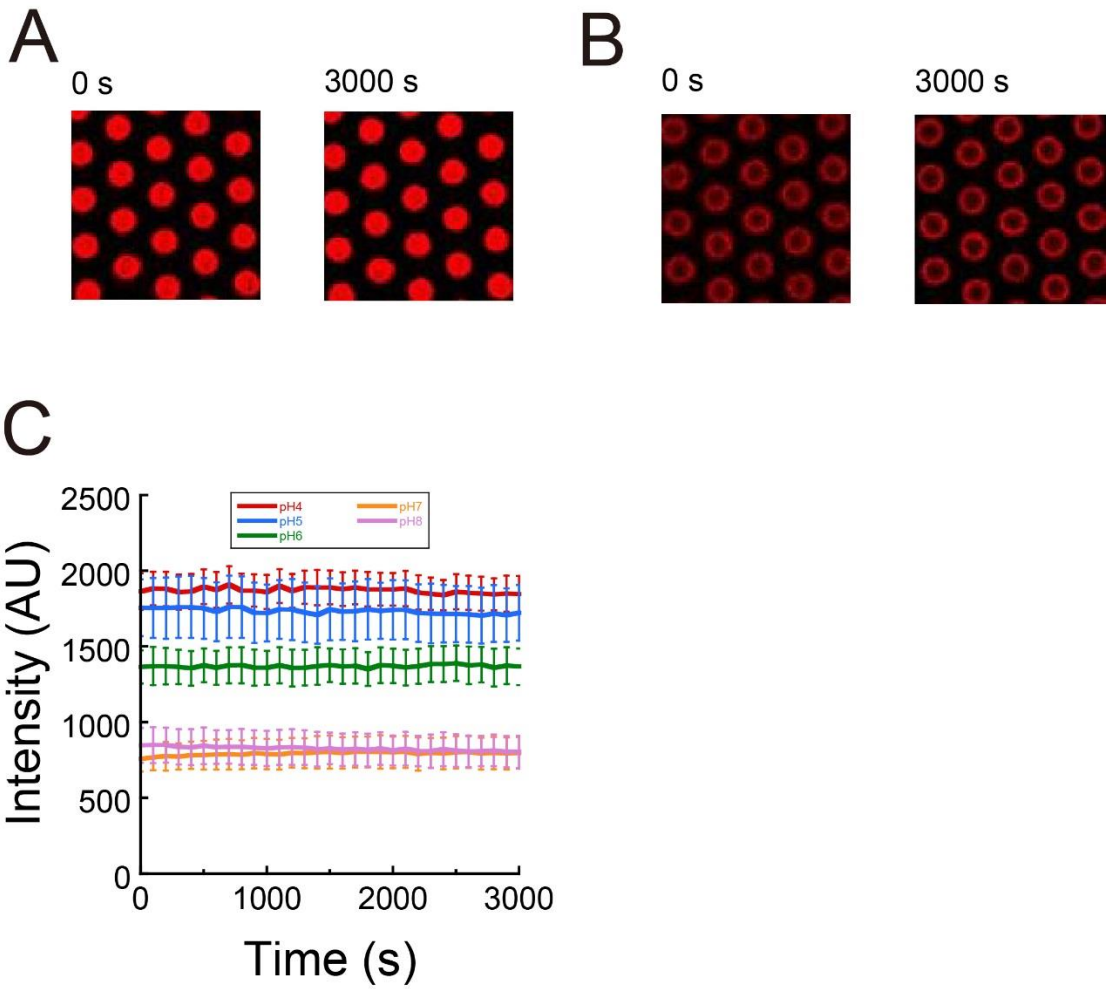

Supplementary Figure 6. Time course of the fluorescent intensity of RhP-M in the chambers

(**A**) Time course of fluorescent images of 10 μM RhP-M at pH 4. (**B**) Time course of fluorescent images of 10 μM RhP-M at pH 8. (**C**) Fluorescent intensity of 10 μM RhP-M in the chambers recorded at pH 4 (red), pH 5 (blue), pH 6 (green), pH 7 (orange), and pH 8 (purple).

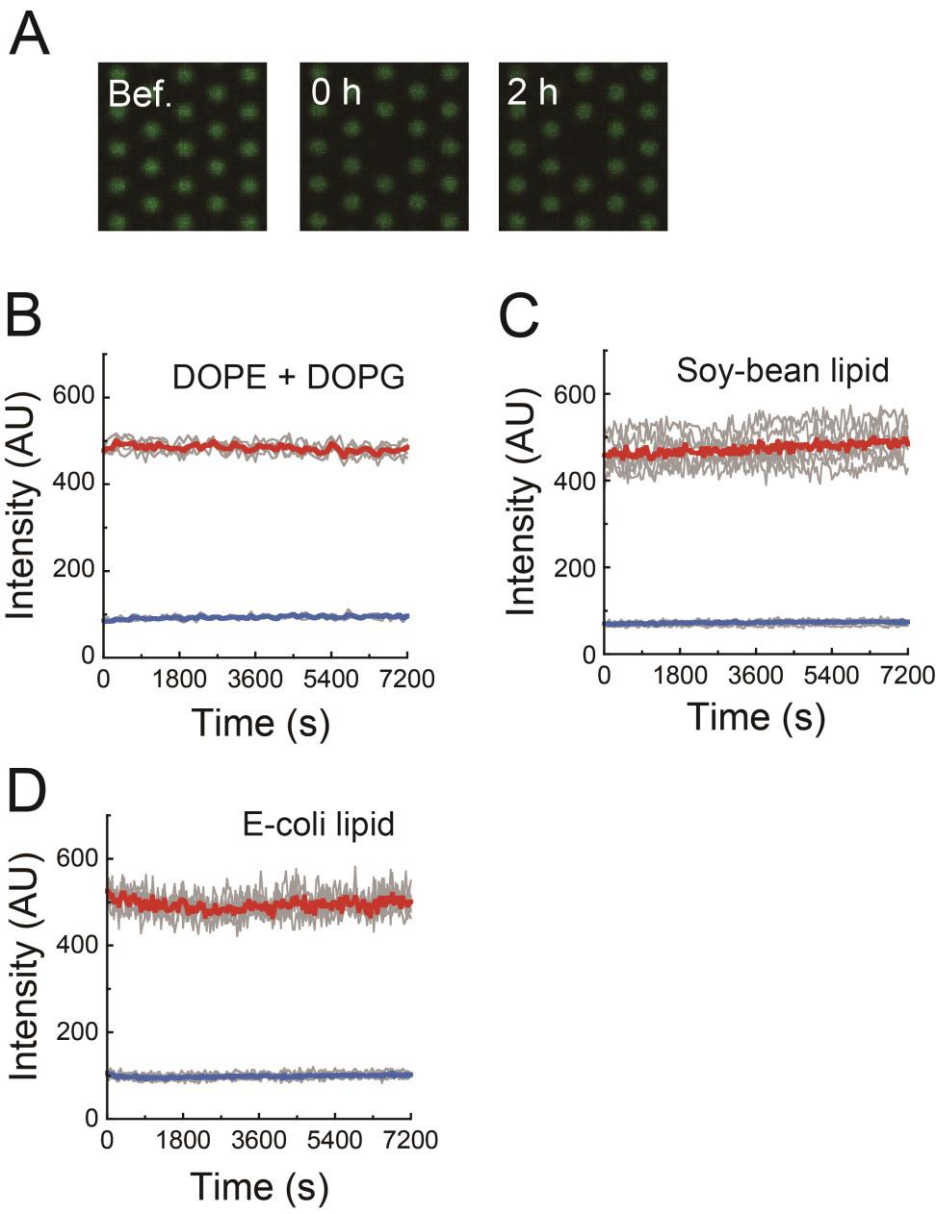

Supplementary Figure 7. FRAP measurement of Alexa 488

(**A**) Fluorescent images of 1 μM Alexa 488 in the chambers recorded before (Bef.) photobleaching (left panel) and at 0 h (middle panel) and 2 h (right panel) after photobleaching. (**B**), (**C**), (**D**), Representative time courses of the fluorescent intensity of the photobleached chambers (blue) and their surrounding chambers (red). Lipid compositions of ALBiC were DOPE and DOPG for (**B**), soy-lipid for (**C**), and E-coli lipid for (**D**).

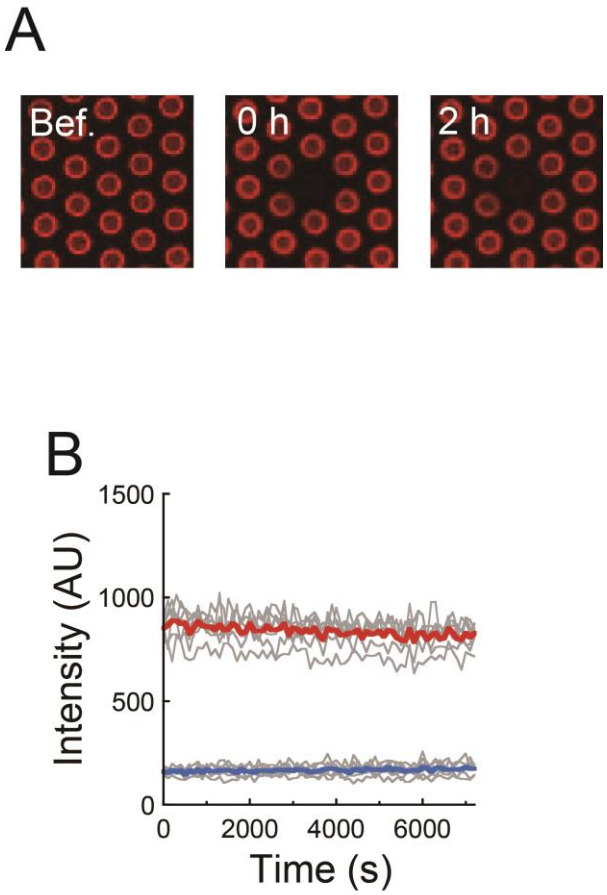

Supplementary Figure 8. FRAP measurement of RhP-M

(**A**) Fluorescent images of 10 μM RhP-M in the chambers recorded before (Bef.) photobleaching (left panel) and at 0 h (middle panel) and 2 h (right panel) after photobleaching. (**B**) Representative time courses of the fluorescent intensity of the photobleached chambers (blue) and their surrounding chambers (red). Lipid composition of ALBiC was DOPE and DOPG.

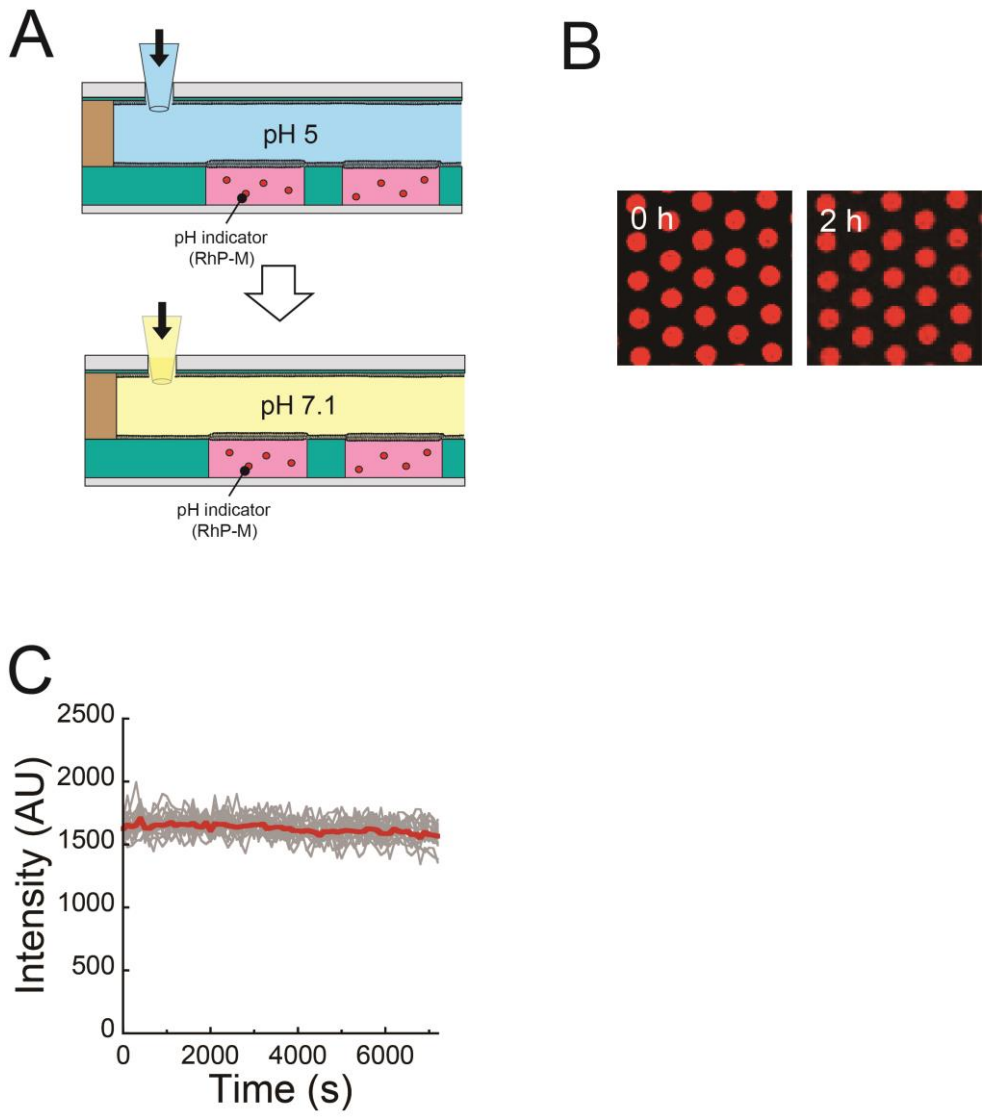

Supplementary Figure 9. Leakage of protons

(**A**) Schematic illustration of the buffer exchange from pH 5 to pH 7.1 after the formation of lipid membranes in nanochambers. Before the buffer exchange, the pH in the chambers was 5. (**B**) Fluorescent images of 10 μM RhP-M before and after buffer exchange. (**C**) Representative time courses of the fluorescent intensity of 10 μM RhP-M after the buffer exchange.

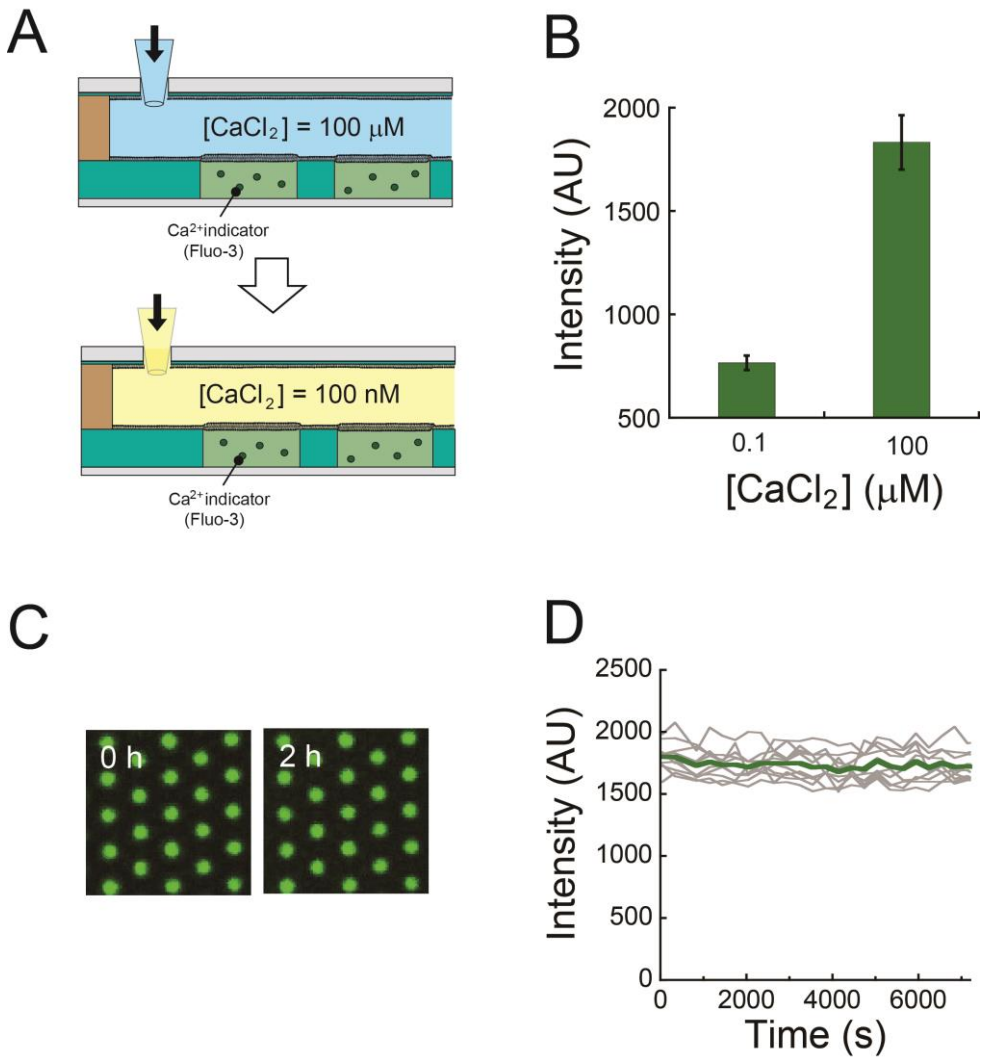

Supplementary Figure 10. Leakage of Ca^{2+}

(**A**) Schematic illustration of the buffer exchange from 100 μM to 100 nM $CaCl_2$ after the formation of lipid membranes on nanochambers. The fluorescent Ca^{2+} indicator, Fluo-3, was encapsulated in each chamber. Before the buffer exchange, [$CaCl_2$] in the chambers was 100 μM. (**B**) Fluorescent intensity of Fluo-3 versus [$CaCl_2$]. (**C**) Fluorescent images of 20 μM Fluo-3 before and after buffer exchange. (**D**) Representative time courses of the fluorescent intensity of 20 μM Fluo-3 after the buffer exchange.

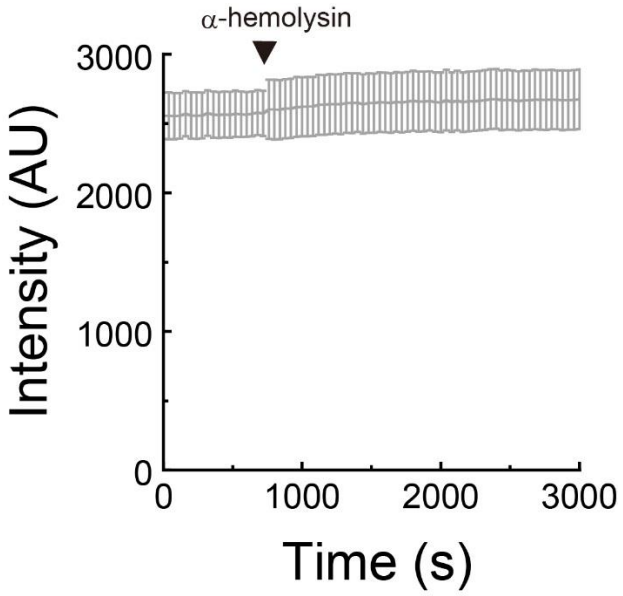

Supplementary Figure 11. Passive transport of Qdot 605 by 1 μg mL^{-1} α-hemolysin

Continuous recording of passive transport activity of Qdot 605 by 1 μg mL^{-1} α-hemolysin. Over the study period, activity was not observed as a continuous decrease in the fluorescence concentration.

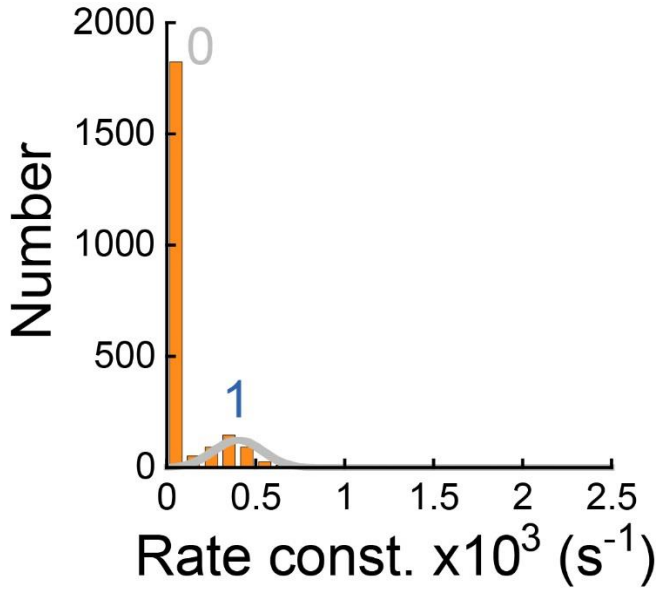

Supplementary Figure 12. Passive transport by 0.1 μg mL^{-1} α-hemolysin

The histogram of passive transport activity by 0.1 μg mL^{-1} α-hemolysin. In this histogram, the number of chambers was plotted versus the rate constant of passive transport. The two peaks can be attributed to occupancies of 0 or 1 α-hemolysin molecules per chamber. The second peak was fitted with a Gaussian curve (gray).

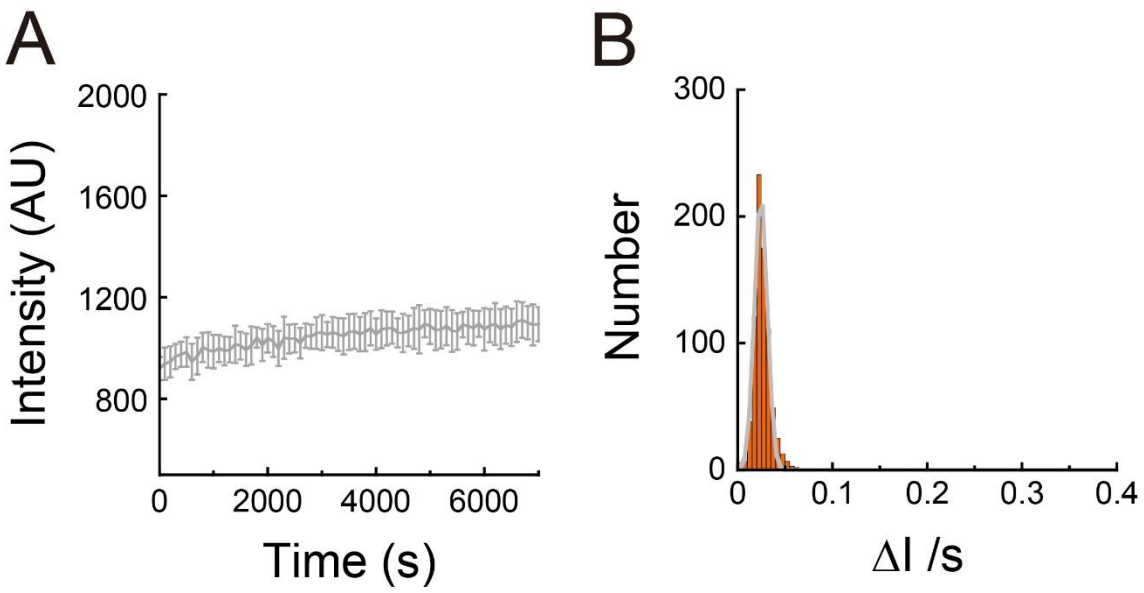

Supplementary Figure 13. Active transport by DCCD-treated F_oF_1-ATP synthase

(**A**) Continuous recording of proton pumping by F_oF_1-ATP synthase treated with 10 μM DCCD for 1 h. (**B**) In the histogram, the number of chambers is plotted versus the slope of fluorescence increments from 1,500 to 4,000 s. The peak was fitted with a Gaussian curve.

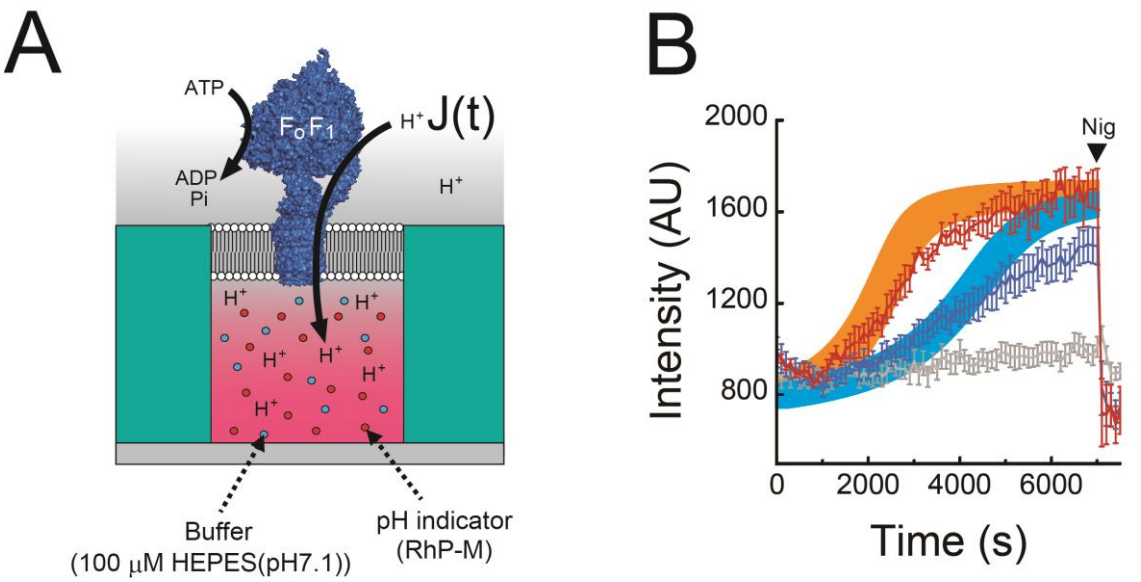

Supplementary Figure 14. Physicochemical model of proton pumping

(**A**) Schematic illustration of the active transport of F_oF_1. F_oF_1 pumps protons from outside to inside the nanochamber by hydrolyzing ATP. Buffer A (pH 7.1) and the fluorescent pH indicator (RhP-M) are encapsulated in the nanochamber. (**B**) Time course of proton pumping monitored by RhP-M. Solid lines represent the fitting curves based on Eq. [9] for a single molecule (cyan) or two molecules of F_oF_1 (orange). The determined proton-pump rates for a single molecule or two molecules of F_oF_1 were 30 and 50 s^{-1}, respectively.